Pergamon

Acta mater. Vol. 45, No. 10, pp. 4145–4154, 1997

Printed in Great Britain
PII: S1359-6454(97)00101-8
1359-6454/97 $17.00 + 0.00

TOPOLOGICAL EVOLUTION DURING COUPLED GRAIN GROWTH AND OSTWALD RIPENING IN VOLUME-CONSERVED 2-D TWO-PHASE POLYCRYSTALS

DANAN FAN and LONG-QING CHEN†

Department of Materials Science and Engineering, The Pennsylvania State University, University park, PA 16802, U.S.A.

(Received 11 September 1996; accepted 13 February 1997)

Abstract—The topological evolution during coupled grain growth and Ostwald ripening in volume-conserved two-phase polycrystalline systems was studied in two dimensions (2-D), employing computer simulations based on a continuum diffuse-interface field model. The topological distributions were found to scale with time, but dependent on the ratios of grain boundary energies to the interphase boundary energy, the volume fractions and the initial microstructures. The correlations between topological class and grain size, as well as the topological correlations of grains with their neighbor grains were observed. The differences in topological features between volume-conserved two-phase systems and single-phase systems are discussed. © *1997 Acta Metallurgica Inc.*

1. INTRODUCTION

The fundamental features of topological evolution in single-phase systems have been extensively investigated because of their importance in understanding the fundamental mechanisms of grain growth [1–9]. However, the topological evolution during coupled grain growth and Ostwald ripening in two-phase polycrystalline materials receives much less attention, partially due to the complexity of topological evolution in two-phase polycrystalline solids. For example, while only trijunctions are stable in a 2-D single-phase solid, both quadrijunctions and trijunctions can be stable in a 2-D two-phase solid [10–12]. The Mullins–Von Neumann law, which relates the change rate of the area to the number of sides of a grain, was found to be valid on the average in a single-phase system [13, 14], whereas there is no reason to believe this is still true in two-phase systems. Even for the simplest case, a two-phase system with exactly the uniform concentration (no diffusion), with isotropic grain boundary and interphase boundary energies, and with only trijunctions, the change of the area for an individual grain is determined by the number of corners, the number of unlike-phase neighbor grains, and the number of switches from one phase to the other around that grain [10]. Moreover, if there are limited mutual solubilities between the two phases, grain growth through grain boundary migration and Ostwald ripening via long-range diffusion are expected to take place simultaneously.

The microstructure stability in volume nonconserved two-phase systems has been studied by Holm *et al.* [11]. While some common features may be found between conserved and nonconserved systems, significant differences exist [12]. Recently, the authors have developed a diffuse-interface field model for simulating the microstructure evolution in volume-conserved two-phase systems [15]. A significant feature of this model is that the microstructural complexity and long-range diffusion in two-phase systems can be taken into account automatically and simultaneously. The microstructural stability and the kinetics of grain growth in volume-conserved two-phase systems have been studied by employing this model [12]. It has been shown that the kinetics of grain growth in a volume-conserved two-phase system is controlled by long-range diffusion, and the average size (R_t) as a function of time (t) follows the power-growth law, $R_t^m - R_0^m = kt$ with $m = 3$, which is independent of the energetic ratios, initial microstructures and volume fractions of two-phases [12].

The main objective of the paper is to study the topological evolution during the diffusion-controlled grain growth in volume-conserved two-phase systems. In particular, we will focus on the topological transformations, the grain side distributions, the correlations between the average grain size and the average grain edges, and the correlations of grain edges with the average edges of their neighbor grains, based on the temporal evolution of microstructures generated from the computer simulations.

†To whom all correspondence should be addressed.

2. THE DIFFUSE-INTERFACE FIELD MODEL

The details about this model have been discussed previously [12, 15]. To describe an arbitrary two-phase polycrystalline microstructure using the diffuse-interface theory, a set of continuous field variables is defined in this model,

$$\eta_1^\alpha(r),\eta_2^\alpha(r),\ldots,\eta_p^\alpha(r),\eta_1^\beta(r),\eta_2^\beta(r),\ldots,\eta_q^\beta(r),C(r), \quad (1)$$

where η_i^α $(i=1,\ldots,p)$ and η_j^β $(j=1,\ldots,q)$ are called orientation field variables with each representing grains of a given crystallographic orientation of a given phase (denoted as α or β). Those variables change continuously in space and assume continuous values ranging from -1.0 to 1.0. $C(r)$ is the composition field which takes the value of C_α within an α grain and C_β within a β grain.

The total free energy of a two-phase polycrystal system, F, is written as

$$F=\int\Big[f_0(C(r);\eta_1^\alpha(r),\eta_2^\alpha(r),\ldots,\eta_p^\alpha(r);\eta_1^\beta(r),\eta_2^\beta(r),\ldots,\eta_q^\beta(r)) + \frac{\kappa_C}{2}(\nabla C(r))^2+\sum_{i=1}^{p}\frac{\kappa_i^\alpha}{2}(\nabla\eta_i^\alpha(r))^2 + \sum_{i=1}^{q}\frac{\kappa_i^\beta}{2}(\nabla\eta_i^\beta(r))^2\Big]d^3r, \quad (2)$$

where ∇C, $\nabla\eta_i^\alpha$ and $\nabla\eta_j^\beta$ are gradients of concentration and orientation fields, κ_C, κ_i^α and κ_i^β are the corresponding gradient energy coefficients, and f_0 is the local free energy density which, in this work, is assumed to be,

$$f_0=f(C)+\sum_{i=1}^{p}f(C,\eta_j^\alpha)+\sum_{i=1}^{q}f(C,\eta_j^\beta) + \sum_{k=\alpha i=1 j=1}^{\beta}\sum^{p}\sum^{q}f(\eta_i^k,\eta_j^k) \quad (3)$$

in which

$$f(C)=-(A/2)(C-C_m)^2+(B/4)(C-C_m)^4+(D_\alpha/4)(C-C_\alpha)^4+(D_\beta/4)(C-C_\beta)^4$$

$$f(C,\eta_j^\alpha)=-(\gamma_\alpha/2)(C-C_\beta)^2(\eta_i^\alpha)^2+(\delta_\alpha/4)(\eta_i^\alpha)^4$$

$$f(C,\eta_j^\beta)=-(\gamma_\beta/2)(C-C_\alpha)^2(\eta_i^\beta)^2+(\delta_\beta/4)(\eta_i^\beta)^4$$

$$f(\eta_i^k,\eta_j^k)=(\varepsilon_{ij}^{kk}/2)(\eta_i^k)^2(\eta_j^k)^2$$

where C_α and C_β are the equilibrium compositions of α and β phases, $C_m=(C_\alpha+C_\beta)/2$, A, B, D_α, D_β, γ_α, γ_β, δ_α, δ_β, and ε_{ij}^{kk} are phenomenological parameters. The parameters are chosen in such a way that f_0 has p degenerate minima with equal depth located at $(\eta_1^\alpha,\ \eta_2^\alpha,\ldots,\eta_p^\alpha)=(1,0,\ldots,0),\ (0,1,\ldots,0),\ldots,(0,0,\ldots,1)$ at the equilibrium concentration C_α, and has q degenerate minima located at $(\eta_1^\beta,\eta_2^\beta,\ldots\eta_q^\beta)=(1,0,\ldots,0),\ (0,1,\ldots,0),\ldots,(0,0,\ldots,1)$ at C_β. This requirement ensures that each point in space can only belong to a grain with a given orientation of a given phase. The justification of using such a free energy model in the study of coarsening was discussed previously [15].

The energy of a planar grain boundary, σ_{gb}^α, between an α-grain of orientation i and another α-grain of orientation j may be calculated as follows,

$$\sigma_{gb}^\alpha=\int_{-\infty}^{+\infty}\Big[\Delta f(\eta_i^\alpha,\eta_j^\alpha,C)+\frac{\kappa_C}{2}\left(\frac{dC}{dx}\right)^2+\frac{\kappa_i^\alpha}{2}\left(\frac{d\eta_i^\alpha}{dk}\right)^2+\frac{\kappa_j}{2}\left(\frac{d\eta_j^\alpha}{dx}\right)^2\Big]dx \quad (4)$$

in which

$$\Delta f(\eta_i^\alpha,\eta_j^\alpha,C)=f_0(\eta_i^\alpha,\eta_j^\alpha,C)-f_0(\eta_{i,e}^\alpha,\eta_{j,e}^\alpha,C_\alpha)-(C-C_\alpha)\left(\frac{\partial f_0}{\partial C}\right)_{\eta_{i,e}^\alpha,\eta_{j,e}^\alpha,C_\alpha} \quad (5)$$

where $f_0(\eta_{i,e}^\alpha,\eta_{j,e}^\alpha,C_\alpha)$ represents the free energy density minimized with respect to η_i^α and η_j^α at the equilibrium composition of α phase C_α. The grain boundary energy for β phase and the interphase energy between α and β grains can be calculated similarly [12, 15].

The evolution of the field variables are described by the time-dependent Ginzburg–Landau (TDGL) and Cahn–Hilliard [16] equations,

$$\frac{d\eta_i^\alpha(r,t)}{dt}=-L_i^\alpha\frac{\delta F}{\delta\eta_i^\alpha(r,t)},\quad i=1,2,\ldots,p, \quad (6a)$$

$$\frac{d\eta_i^\beta(r,t)}{dt}=-L_i^\beta\frac{\delta F}{\delta\eta_i^\beta(r,t)},\quad i=1,2,\ldots,q, \quad (6b)$$

$$\frac{dC(r,t)}{dt}=\nabla\left\{L_C\nabla\left[\frac{\delta F}{\delta C(r,t)}\right]\right\} \quad (6c)$$

where L_i^α, L_i^β and L_C are kinetic coefficients related to grain boundary mobilities and atomic diffusion coefficients.

In this paper, the kinetic equations for a concentration field and two sets of orientation variables were numerically solved. All the results discussed below were obtained by using the finite-difference method and by assuming $\Delta x=2.0$, $\Delta t=0.1$. The kinetic equations are discretized using 256×256 or 512×512 points with periodic boundary conditions applied along both directions. The total number of orientation field variables for two phases is 30.

For starting a computer simulation, one may either input a pre-defined initial two-phase microstructure or a liquid or disordered phase at a very high temperature. Because we can always normalize the length scale and time scale of kinetic equations with diffusion coefficients and boundary mobilities, we simply choose $L_\eta^\alpha=L_\eta^\beta=1.0$ (isotropic grain boundary mobility) and $L_c=0.5$, implying that the two phases have the same diffusion coefficients and

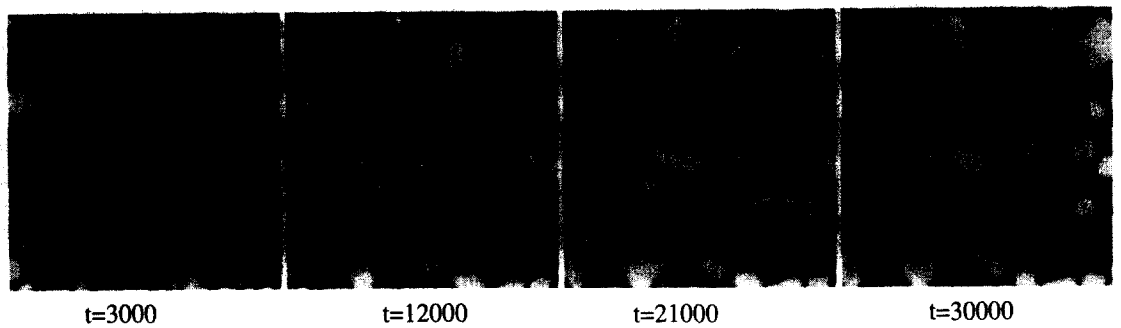

Fig. 1. The microstructural evolution in a system with $R_\alpha = R_\beta = 1.0$. The volume fraction of the α phase is 50%. System size is 256 × 256.

boundary mobilities. We also assumed isotropic grain boundary energies for both phases and an isotropic interphase boundary energy between α and β phase, i.e., $\kappa_i^\alpha = \kappa_j^\alpha = \kappa^\alpha$ and $\kappa_i^\beta = \kappa_j^\beta = \kappa^\beta$. Furthermore, we assumed that the solubilities in the α and β phase are: $C_\alpha = 0.05$ and $c_\beta = 0.95$. The gradient energy coefficients and phenomenological parameters in the free energy function were fitted to grain boundary energies, interfacial energy and their ratios to give the desired energetic conditions in the simulation.

To calculate individual grain size, a cut-off value of orientation fields was chosen, which clearly defines the grain boundaries and neighbors of grains. The area of each grain at a given time step is directly calculated from the microstructure by counting the number of grid points within a grain and grain size R is obtained from the area A by assuming a circular shape for all grains, therefore, $A = \pi R^2$. The average grain radius at a given time step is then obtained by averaging over all the grains in a system.

3. TOPOLOGICAL EVOLUTION IN $R_\alpha = R_\beta$ SYSTEMS

Thermodynamically, the microstructural features in a two-phase system can be characterized using the energetic ratios of grain boundary energies to the interphase boundary energy, R_α and R_β: $R_\alpha = \gamma_\alpha/\gamma_{\alpha\beta}$, $R_\beta = \gamma_\beta/\gamma_{\alpha\beta}$, where γ_α is the grain boundary energy in α phase, γ_β is the grain boundary energy in β and $\gamma_{\alpha\beta}$ is the interphase boundary energy between α and β. These energetic ratios can be related to dihedral angles as: $2\cos[\phi_\beta/2] = R_\alpha$ and $2\cos[\phi_\alpha/2] = R_\beta$, where ϕ_β is the dihedral angle formed by two α grains and a β grain, and ϕ_β is the angle formed by two β grains and an α grain. It was shown that [10–12], for $0 \le R_\alpha \le \sqrt{3}$, $\alpha\alpha\alpha$ trijunctions are stable, and when $R_\alpha > \sqrt{3}$, $\alpha\alpha\alpha$ trijunctions are unstable with respect to the nucleation of β grains. Similarly, $\beta\beta\beta$ trijunctions are stable for $0 \le R_\beta \le \sqrt{3}$ and are unstable with respect to the nucleation of α grains for $R_\beta > \sqrt{3}$. $\alpha\alpha\beta$ and $\alpha\beta\beta$ trijunctions are stable under the conditions of $0 \le R_\alpha > 2$ and $0 \le R_\beta > 2$, respectively. The quadrijunctions $\alpha\beta\alpha\beta$ will become stable for $R_\alpha^2 + R_\beta^2 \ge 4$ [10–12].

The simplest case is $R_\alpha = R_\beta = 1$, in which the interphase boundary energy between α and β is equal to the grain boundary energies in α and β. In this case, $\alpha\alpha\alpha$, $\alpha\alpha\beta$, $\alpha\beta\beta$ and $\beta\beta\beta$ trijunctions are thermodynamically stable and equally favored. An example of microstructural evolution is shown in Fig. 1. The topological transformations during grain growth are similar to those in single-phase materials. The average sides per grain is 5.999, which is essentially the same as that in single phase systems. The topological distributions at different time steps are shown in Fig. 2 for both α and β grains. From Fig. 2, it seems that a scaling state has been reached for topological distributions. However, the peaks of the distributions are located at 6-sided grains, comparing to single-phase systems in which the peaks are at 5-sided [12, 18–20]. The only difference between a two-phase system with $R_\alpha = R_\beta = 1$ and a single-phase system with isotropic grain boundary energies is the fact that the kinetics of grain growth and topological evolution in single-phase systems are driven by the boundary mean-curvatures, whereas in

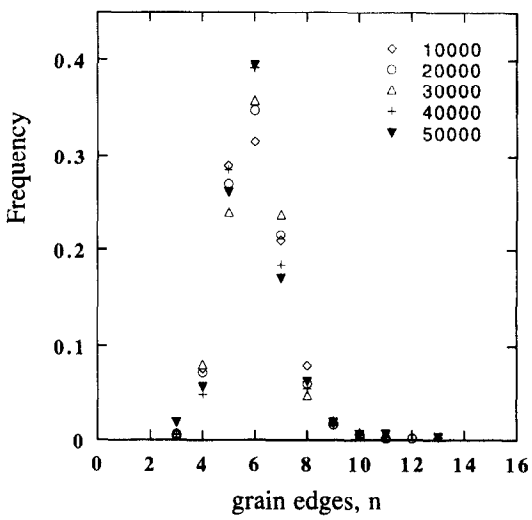

Fig. 2. The time dependence of topological distributions in the system with $R_\alpha = R_\beta = 1.0$ for both α and β phases. The volume fraction of α phase is 50%. Time step = 10000, 20000, 30000, 40000, 50000.

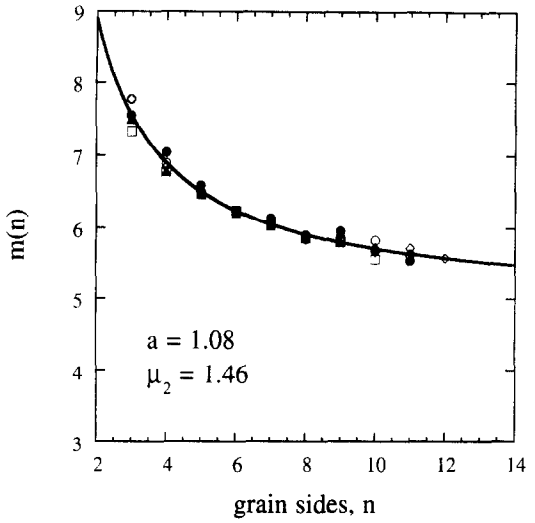

Fig. 3. The neighbor side correlation function $m(n)$ at different time steps. The solid line is a fit to the Aboav–Weaire law with $a = 1.08$ and $\mu_2 = 1.46$. $R_\alpha = R_\beta = 1.0$. The volume fraction of the α phase is 50%.

volume-conserved two-phase systems the interface motion is controlled by the long-range diffusion. It is interesting that the kinetic mechanisms alone can affect the shape of topological distributions. It was also shown that the peak of topological distributions may vary as neighbors of two phase grains change in non-conserved two-phase systems [11].

In single-phase systems, a correlation function between the number of sides n of a grain and the average sides of its neighbors, $m(n)$, is given by Aboav–Weaire law [21, 22]

$$m(n) = 6 - a + \frac{6a + \mu_2}{n}, \tag{7}$$

where μ_2 is the second moment of the side distribution and a is a constant. To examine if a similar topological correlation exists in two-phase systems, the $m(n)$ values calculated at different time steps for the system $R_\alpha = R_\beta = 1.0$ are shown in Fig. 3. It is clear that few-sided grains prefer to be surrounded by many-sided grains, and vice versa, i.e., correlation between grains exists in two-phase systems. It is found that the Aboav–Weaire law, which was originally proposed for single-phase grain growth, can describe the data very well with $a = 1.08$ and $\mu_2 = 1.46$. The μ_2 value is consistent with that calculated directly from topological distributions.

Feltham [23] predicted a linear relationship between the average grain radius of n-sided grains, $\langle R_n \rangle$, with topological class, n, for grain growth in single-phase systems, i.e.,

$$\langle R_n \rangle = \beta'(n - n_0), \tag{8}$$

where β' and n_0 are constants. Similar correlation between grain size and topological class n seems to exist in this two-phase system. Figure 4 shows the relationship between topological class and average grain size in each topological class for the α phase. In this plot, a normalized grain size $\langle R_n \rangle / \langle R \rangle$ is used to compare the results at different time steps, where $\langle R \rangle$ is the average grain size for all of the grains of that phase at a certain time step. It is shown that, on the average, the number of sides of a grain increases linearly with its size. This linear relationship is time-invariant and identical in both phases with $\beta' = 0.186$ and $n_0 = 0.62$ in this system.

We also studied a system with $R_\alpha = R_\beta = 2.1$ in which the microstructures are comprised entirely of quadrijunctions (Fig. 5). The topological events observed in this system are very different from those found in single-phase grain growth and those in two-phase systems with only trijunctions. It is observed that grains with two quadrijunctions and grains with three quadrijunctions can vanish during coarsening. The vanishing of a grain with two quadrijunctions, which is surrounded by two grains of the other phase separated by two interphase boundaries plus two grains of the same phase separated by two quadrijunctions, brings four grains (two of each phase) together, resulting in the disappearance of two quadrijunctions and the formation of a new quadrijunction. During this process, the two neighbor grains, which were separated from the vanishing grain by interphase boundaries, lose one side each. The vanishing of three quadrijunction grains results in six grains (three of each phase) coming together to form a hexajunction, which is highly unstable and quickly splits into two new quadrijunctions. The result is that each of the two adjacent grains of the other phase loses one side and one of the same phase grains gains one side with the rest of the neighbor grains remaining unchanged.

Despite the dramatic differences in topological transformations between all-quadrijunction and all-

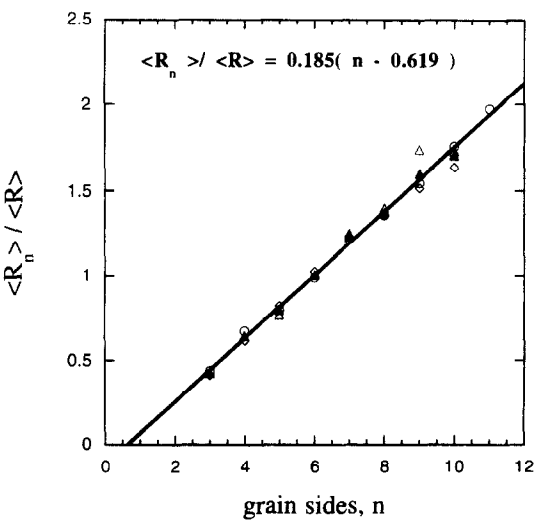

Fig. 4. The correlation between the average grain size in a given topological class and the topological class n in the α phase at different time steps. $R_\alpha = R_\beta = 1.0$. The volume fraction of the α phase is 50%.

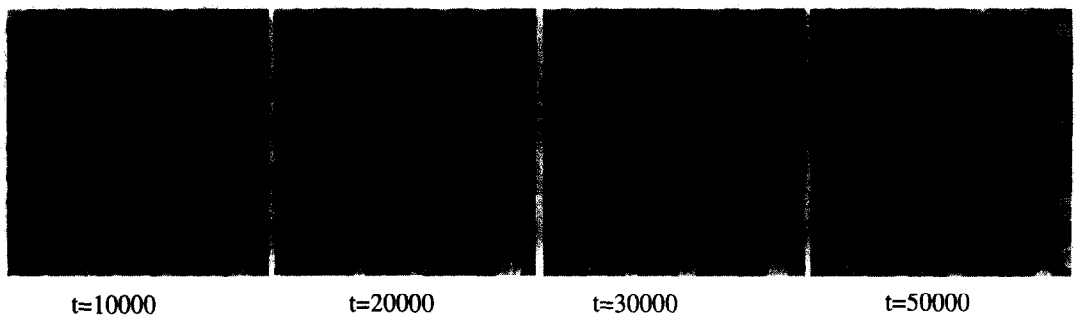

Fig. 5. The microstructural evolution in a system with $R_\alpha = R_\beta = 2.1$. The volume fraction of α phase is 50%. System size is 256 × 256.

trijunction systems, their topological distributions are similar. For example, the distributions scale with time and peaks occur at 6-sided grains (Fig. 6 and Fig. 2) in both systems. However, the distributions are wider and the average number of grain sides is 5.92 in the all-quadrijunction system as a result of the existence of a significant number of 2-sided grains.

The correlations of grains with neighbor grains and the correlations of grain size with topological class, n, were also examined (Fig. 7 and Fig. 8). Similar to the all-trijunction system and single-phase grain growth, the Aboav-Weaire law and Feltham law describe the correlations quite well in the all-quadrijunction system. One noticeable difference is that the value of the second moment μ_2 of toplogical distributions is 2.19, which is larger than $\mu_2 = 1.46$ for the system with $R_\alpha = R_\beta = 1.0$. The higher value of the second moment μ_2 is consistent with the wider topological distributions and is a result of relative high frequencies of many-sided grains and two-sided grains [12, 24].

4. TOPOLOGICAL EVOLUTION IN $R_\alpha \neq R_\beta$ SYSTEMS

A specific system, Al_2O_3-ZrO_2 two-phase composite, is chosen as an example to study the topological evolution for $R_\alpha \neq R_\beta$. In this case, grain boundaries in the α phase are no longer equivalent to grain boundaries in β. In Al_2O_3-ZrO_2, it was reported [25, 26] that the average ratio of grain boundary energy to the interphase energy for the Al_2O_3 phase (denoted as α phase) is: $R_\alpha = \sigma^{\alpha}_{alu}/\sigma^{\alpha\beta}_{int} = 1.4$, and the ratio for the ZrO_2 phase (denoted as β phase) is: $R_\beta = \sigma^{\beta}_{zir}/\sigma^{\alpha\beta}_{int} = 0.97$. In this system, $R_\alpha = 1.4 < \sqrt{3}$, $R_\beta = 0.97 < 1$ and $R_\alpha^2 + R_\beta^2 = 2.9 < 4$. Therefore, in 2-D, all trijunctions are thermodynamically stable while no quadrijunctions are stable.

Since the grain boundary energy of Al_2O_3 is much higher than that of ZrO_2 ($R_\alpha = 1.4$, $R_\beta = 0.97$), thermodynamic equilibrium angles at the trijunctions formed by two α grains and a β grain ($\alpha\alpha\beta$) are different from those formed by one α grain and two β grains ($\alpha\beta\beta$). At an $\alpha\beta\beta$ trijunction, the equilibrium angle (ϕ_α) α is given by: $2\cos(\phi_\alpha/2) = R_\beta$, which gives $\phi_\alpha = 121.98°$, whereas the equilibrium angle in β at

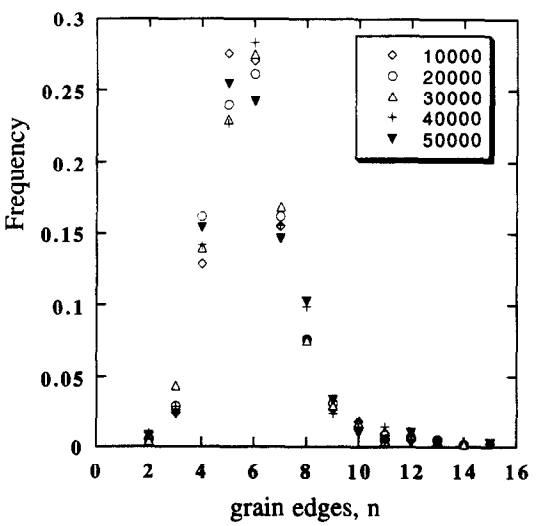

Fig. 6. The time dependence of topological distributions in the system with $R_\alpha = R_\beta = 2.1$ for both α and β phases. The volume fraction of the α phase is 50%. Time step = 10000, 20000, 30000, 40000.

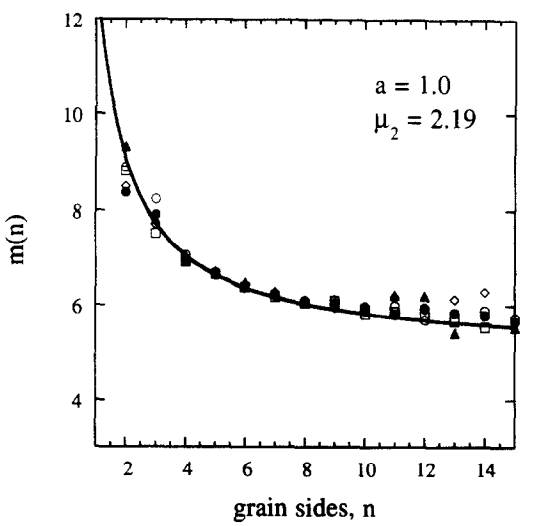

Fig. 7. The neighbor-side correlation function $m(n)$ at different time steps. The solid line is a fit to the Aboav-Weaire law with $a = 1.0$ and $\mu_2 = 2.19$. $R_\alpha = R_\beta = 2.1$. The volume fraction of the α phase is 50%.

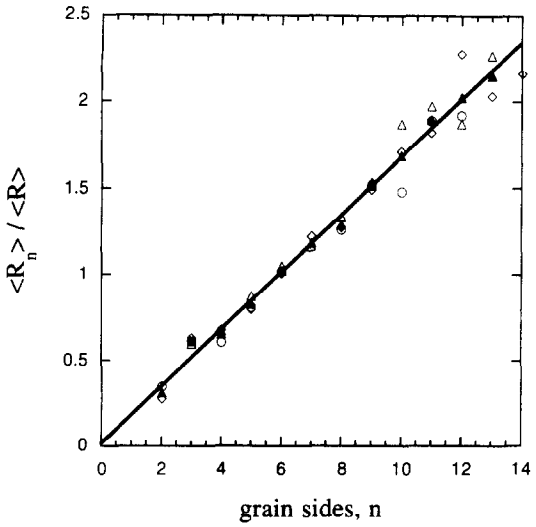

Fig. 8. The correlation between grain size and topological class n in the α phase at different time steps. $R_\alpha = R_\beta = 2.1$. The volume fraction of the α phase is 50%.

trijunctions $\alpha\alpha\beta$, ϕ_β, is $2\cos(\phi_\beta/2) = R_\alpha$ and $\phi_\beta = 91.19°$. Because of this difference, an isolated Al_2O_3 (α) grain (surrounded by ZrO_2 grains) will have convex boundaries if the number of grain edges are equal to or less than 6. On the other hand, an isolated ZrO_2 (β) grain is concave until the number of grain edges is less than 4. These phenomena are very different from those in single-phase grain growth, in which grains with less than 6 edges are convex.

From Fig. 9, it can be seen that isolated ZrO_2 (bright) grains with 4 and more edges, in most cases, have concave boundaries, which is consistent with thermodynamic analysis. However, some isolated ZrO_2 grains have mixed concave and convex boundaries and the direction of curvatures can change during the microstructural evolution, even though they have more than 4 edges. This can be clearly seen from the evolution of the grain labeled A in Fig. 9. This grain initially has six concave edges and transforms to a 5-sided and then 4-sided grain with mixed concave and convex boundaries. There are two reasons responsible for the departure of microstructure features from thermodynamic predictions. First, the balance of surface tension only requires the balance of tangents of those curves meeting at a trijunction, hence, the balance can be accomplished by either concave curves and/or convex curves as long as the tangents of these curves give the same angle at the trijunction. Secondly, the topological change of this β grain is due to the coarsening of the neighboring α grains, which results in the shape change and the mass redistribution of this β grain to accommodate the space-filling requirement. The mass redistribution requires the diffusion of atoms along the interfaces or volume diffusion, which is driven by the chemical potential difference at boundaries with different curvatures within this β grain, i.e., atoms at concave boundaries diffuse to convex boundaries because of the shape adaptation. Hence, it is the local shape adjustment and mass redistribution that lead to the formation of mixed concave and convex boundaries. It should be noted that the area of this β grain changes very slowly because the process is governed by the long distance diffusion or Ostwald ripening while the topological transformation and mass redistribution occur quite rapidly, and are controlled by local diffusion.

Another important topological feature in this system is that there is a tendency to eliminate Al_2O_3 grain boundaries because of the higher grain boundary energy in Al_2O_3. One way to eliminate Al_2O_3 grain boundaries is by coarsening or grain growth of Al_2O_3 grains. However, if Al_2O_3 grain boundaries are pinned by ZrO_2 grains, the second mechanism, grain boundary switching, will occur. This can be seen from evolution of grains in Fig. 10 labeled as B. In this region, an initial grain boundary of Al_2O_3 grains is replaced by a grain boundary of ZrO_2 grains to reduce the free energy of the system during microstructural evolution. The driving force for this grain boundary switching is the grain boundary energy difference between two phases. This is very different from the grain boundary switching occurring in single-phase grain growth with isotropic grain boundary energies, in which the driving force is mean curvatures and the grain boundary between two

Fig. 9. The microstructural evolution in the Al_2O_3–10% ZrO_2 system with $R_\alpha = 1.4$ and $R_\beta = 0.97$. System size is 256 × 256.

Fig. 10. The microstructural evolution in the Al_2O_3–20% ZrO_2 system with $R_\alpha = 1.4$ and $R_\beta = 0.97$. System size is 256 × 256.

smaller grains will disappear during grain boundary switching. As the volume fraction of ZrO_2 increases, the Al_2O_3 grains become increasingly isolated by ZrO_2 grains.

The topological distributions of the α and β phases at different time steps are shown in Fig. 11 and Fig. 12 for the 50% ZrO_2 system. Scaling behaviors are observed for both phases. However, the Al_2O_3 phase has a peak at the 6-sided grains while ZrO_2 phase has a peak at the 5-sided grains, which is quite surprising since the only difference between α and β is the energetic ratios ($R_\alpha = 1.4$, $R_\beta = 0.97$). The topological distributions for the α and β phases in the 10% ZrO_2 system are compared in Fig. 13. The distributons are also time-invariant, but the shapes of distributions for α and β phase are very different. It can be seen that the second phase (10% ZrO_2) has much narrower distributions and the peaks have shifted to the 4-sided grain while the distributions for the matrix phase (90% Al_2O_3) are much wider with the peaks still at the 6-sided grains (Fig. 13).

The effect of volume fractions on topological distributions of the ZrO_2 phase is summarized in Fig. 14. It shows that, as the volume fraction of ZrO_2 increases, topological distributions become wider and peak frequencies are lower, accompanied by a shift of the peak position from 4 to 5-sided grains. A similar behavior is also observed at the ZrO_2-rich systems except that in the 10% Al_2O_3 system topological distributions have peaks at the 3-sided grain for the Al_2O_3 phase, which shift to the 6-sided as the volume fraction of Al_2O_3 increases. Similar dependence of topological distributions on volume fractions were observed experimentally on 2-D cross-sections of 3-D microstructures in the Al_2O_3-ZrO_2 two-phase composites [27]. It should be noted that the topology of 2-D system is not necessary to be equivalent to that of a 3-D cross-section, even though the stability criteria for 2-D grain junction are the same as those for 3-D grain edge and the topology of single-phase 2-D systems has a strong similarity to that of cross-sections of 3-D systems [28].

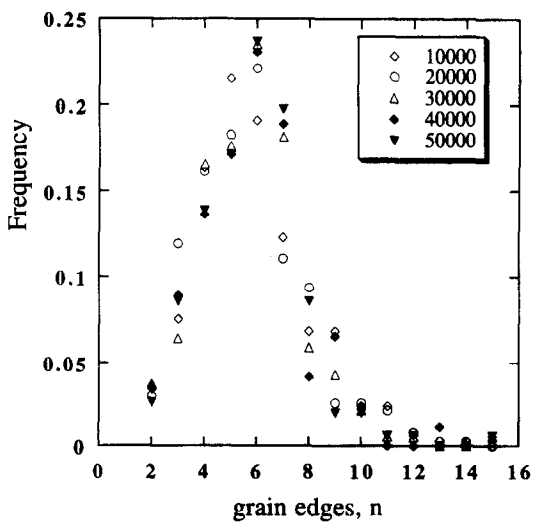

Fig. 11. The time dependence of topological distributions in the Al_2O_3 phase. The volume fraction of ZrO_2 phase is 50%. $R_\alpha = 1.4$, $R_\beta = 0.97$.

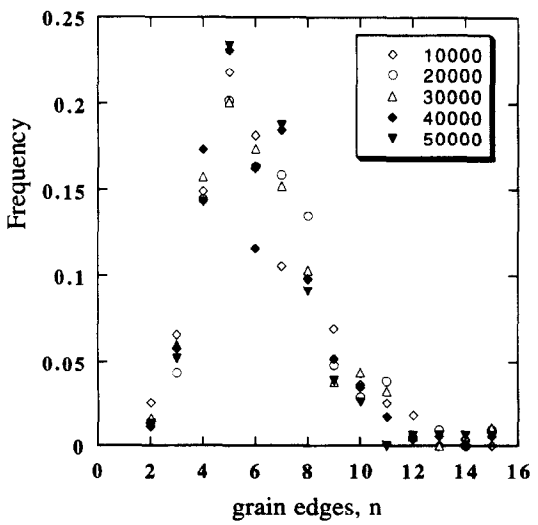

Fig. 12. The time dependence of topological distributions in the ZrO_2 phase. The volume fraction of ZrO_2 phase is 50%. $R_\alpha = 1.4$, $R_\beta = 0.97$.

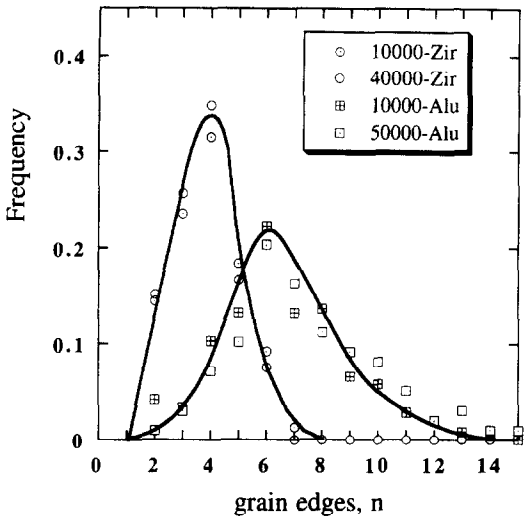

Fig. 13. Comparison of topological distributions of the Al_2O_3 and ZrO_2 phase in the system with 90% Al_2O_3 and 10% ZrO_2. $R_\alpha = 1.4$, $R_\beta = 0.97$.

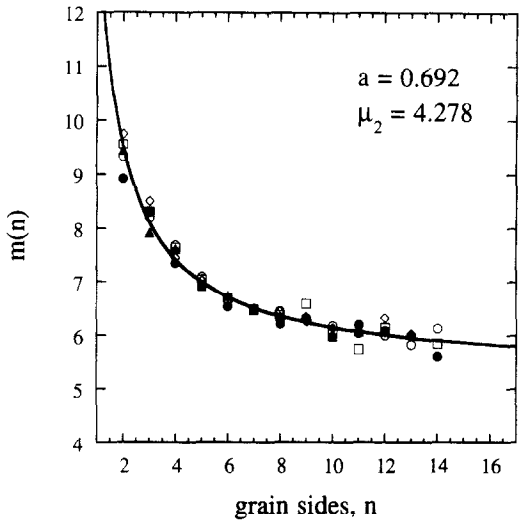

Fig. 15. The topological correlations of grains with their neighbor grains (function $m(n)$) in the 50% ZrO_2 system at different time steps.

The topological correlations of grains with their neighbor grains (Aboav–Weaire law) are observed at all volume fractions. An example is shown in Fig. 15 for the 50% ZrO_2 case. One may notice the large value of the second moment μ_2 (4.28) which comes directly from high frequencies of the occurrence of 2-sided grains and many-sided grains. The average grain edges are 5.38 in the 10% ZrO_2 system and are 5.97 in the 50% ZrO_2 system.

The correlations between grain size and topological class n (Feltham law) were examined. Figures 16 and 17 show the relations between topological class n and normalized average grain size $\langle R_n \rangle / \langle R \rangle$ in each topological class in the 10% and 50% ZrO_2 systems at different time steps. In these two plots, the linear relationship $\langle R_n \rangle = \beta'(n - n_0')$ is observed for both phases at different volume fractions and is time-invariant in all cases. At a certain volume fraction, the slopes of this relation for the two phases are quite similar, but the constants n_0' are different for the two phases. We found that both constants β' and n_0' depend on the volume fractions of the second phase.

The effects of initial microstructures on the topological distributions are compared in Fig. 18 for the α phase and Fig. 19 for the β phase in the 40% ZrO_2 system. In these plots, the solid lines are the topological distributions obtained from initial microstructures generated from direct crystallization of a liquid, and the dashed lines represent the distributions obtained from an initially fine single-phase grain structure produced by a normal grain growth simulation and then by randomly assigning all the grains to either α or β according to the desired volume

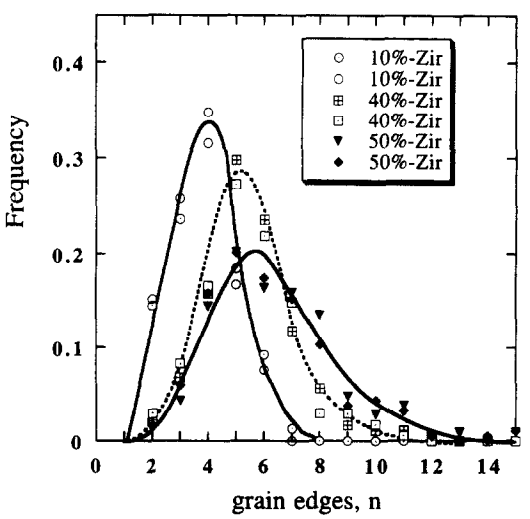

Fig. 14. The effect of volume fractions on the topological distributions in the ZrO_2 phase. $R_\alpha = 1.4$, $R_\beta = 0.97$.

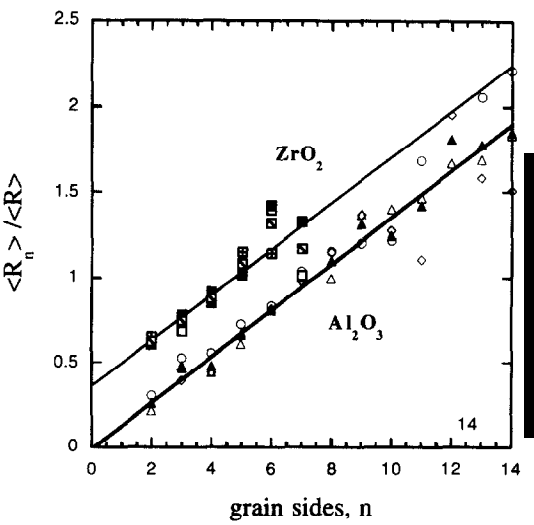

Fig. 16. The correlations between average grain size in a topological class and the topological class n for 10% ZrO_2 at different time steps.

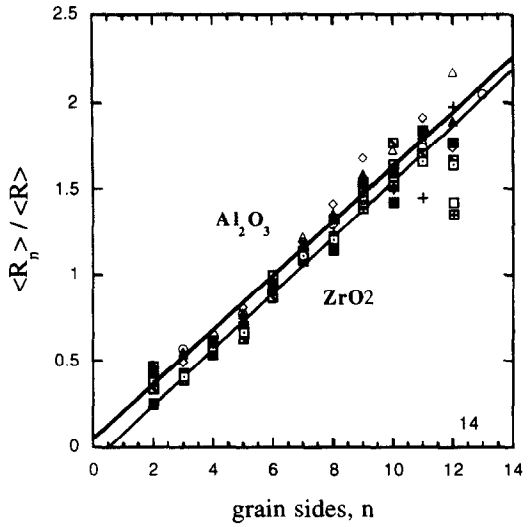

Fig. 17. The correlations between average grain size in a topological class and the topological class n for 50% ZrO_2 at different time steps.

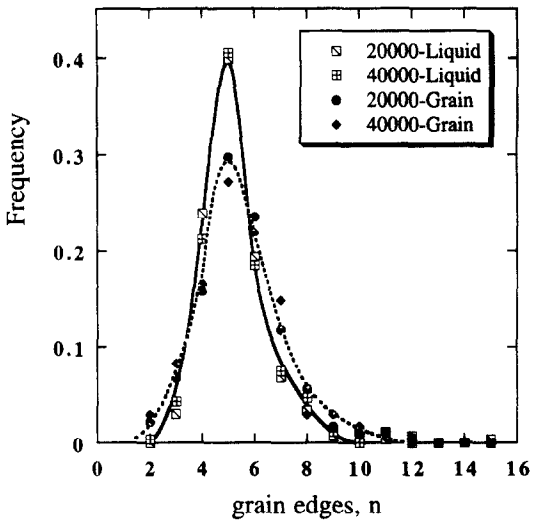

Fig. 19. The effects of initial microstructures on the topological distributions of the ZrO_2 phase in the system with the 40% ZrO_2.

fractions. It can be seen that, if the initial microstructures are generated from a liquid, topological distributions are much sharper and narrower than those obtained from the initial structures generated from a fine grain structure for both phases. However, the peak positions of topological distributions are independent of the initial microstructures, which are located at the 6-sided grain for the Al_2O_3 phase and at the 5-sided grain for the ZrO_2 phase in all cases. Therefore, initial microstructures will affect the shapes of topological distributions, but not the peak positions of topological distributions.

5. CONCLUSIONS

The topological evolution in volume-conserved two-phase systems is studied by computer simulations employing a diffuse-interface field model. The topological features were found to depend on the energetic ratios, volume fractions and initial microstructures, even though they scale with time in all cases. Unique topological transformations in two-phase systems are identified as compared to those in single-phase systems. The correlations between topological class and grain size as well as the topological correlations of grains with their neighbor grains were observed in all cases. The topological features observed in experiments, such as the tendency to eliminate grain boundaries of Al_2O_3 phase during microstructural evolution and the shift of topological distribution peaks from 4-sided grain uto 5-sided grain for ZrO_2 phase with increasing volume fraction of the ZrO_2 phase, were predicted by the computer simulations.

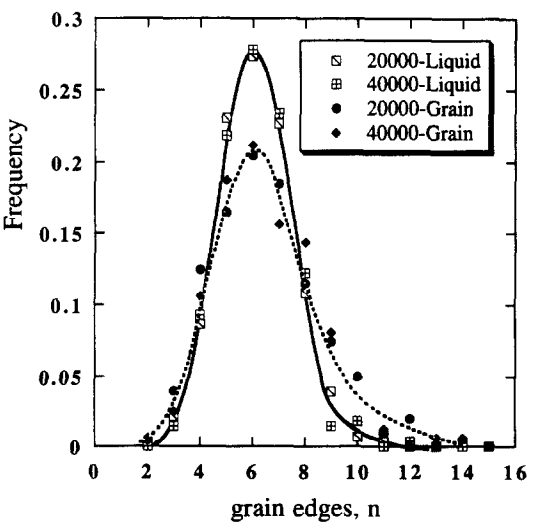

Fig. 18. The effects of initial microstructures on the topological distributions of the Al_2O_3 phase in the system with the 40% ZrO_2.

Acknowledgements—The authors are grateful to Dr K. B. Alexander for providing us with a copy of her short-course notes given at the 1995 ACerS Annual Meeting. This work is supported by NSF under the grant numbers DMR 93-11898 and DMR 96-33719. The computing time was provided by the Pittsburgh Supercomputing Center under the Grant No. DMR 940015P.

REFERENCES

1. Atkinson, H. V., *Acta Metall.*, 1988, **36**, 469, and references therein.
2. Abbruzzese, G., Heckelmann, I. and Lücke, K., *Acta Metall.*, 1992, **40**, 519.
3. Lücke, K., Heckelmann, I. and Abbruzzese, G., *Acta Metall.*, 1992, **40**, 533.
4. Fradkov, V. E., *Phil. Mag. Lett.*, 1988, **58**, 271.
5. Beenakker, C. V. J., *Phys. Rev. Lett.*, 1986, **57**, 2454.
6. Glazier, J. A., Gross, S. P. and Stavans, J., *Phys Rev. A*, 1987, **36**, 306.
7. Mullins, W. W., *J. Appl. Phys.*, 1986, **59**(4), 1341.
8. Glazier, J. A. and Weaire, D., *J. Phys.: Condens. Matter*, 1992, **4**, 1867.
9. Danan Fan, Geng, C. W. and Chen, L.-Q., accepted in *Acta Mater.*, 1997, **45**, 1115.

10. Cahn, J. W., *Acta Metall. Mater.*, 1991, **39,** 2189.
11. Holm, E. A., Srolovitz, D. J., Cahn, J. W., *Acta Metall. Mater.*, 1993, **41,** 1119.
12. Danan Fan and Chen, L.-Q., accepted in *Acta Mater.*, 1997.
13. Mullins, W. W., *J. Appl. Phys.*, 1986, **59**(4), 1341.
14. von Neumann, J., *Metal Interfaces*. ASM, Cleveland, OH, 1952, p. 108.
15. Chen, L.-Q. and Danan Fan, *J. Am. Ceram. Soc.*, 1996, **79,** 1163.
16. Allen, S. M. and Cahn, J. W., *Acta Metall.*, 1979, **27,** 1085.
17. Cahn, J. W., *Acta Metall.*, 1961, **9,** 795.
18. Srolovitz, D. J., Anderson, M. P., Sahni, P. S. and Grest, G. S., *Acta Metall.*, 1984, **32,** 793.
19. Glazier, J. A., *Phil. Mag. B*, 1990, **62,** 615, and references therein.
20. Fradkov, V. E., Shvindlerman, L. S. and Udler, D. G., *Scripta Metall.*, 1985, **19,** 1285.
21. Aboav, D. A., *Metallography*, 1970, **3,** 383.
22. Weaire, D., *Metallography*, 1974, **7,** 157.
23. Feltham, P., *Acta Metall.*, 1957, **5,** 97.
24. Danan Fan, Ph.D. dissertation, The Pennsylvania State University, 1996.
25. I-Wei Chen. and Xue, L. A., *J. Am. Ceram. Soc.*, 1990, **73,** 2585.
26. Lee, G. and Chen, I-W., *Sintering '87, Proceedings of the 4th International Symposium on Science and Technology of Sintering*, Tokoyo, Japan, 1987, ed. Shigeyuki Somiya, Masahiko Shimada, Masahiro Yoshimura, Ryuzo Watanaba. Elsevier Applied Science, London, 1988, Vol. 1, pp. 340–346.
27. Alexander, K. B., Grain Growth and Microstructural Evolution in Two-Phase Systems: Alumina/Zirconia Composites, Short Course on Sintering of Ceramics at the American Ceramic Society Annual Meeting, Cincinnati, OH, April 1995.
28. Anderson, M. P., Grest, G. S. and Srolovitz, D. J., *Phil. Mag. B*, 1989, **59,** 293.